Insights into the mechanism of photosynthetic H 2 evolution catalyzed by a heptacoordinate cobalt complex

Fiorella Lucarini, Jennifer Fize, Adina Morozan, Marco Marazzi, Mirco Natali, Mariachiara Pastore, Vincent Artero, Albert Ruggi

ARTICLE

Insights into the mechanism of photosynthetic H_2 evolution catalyzed by a heptacoordinate cobalt complex

Fiorella Lucarini,[a] Jennifer Fize,[b] Adina Morozan,[b] Marco Marazzi,[c,d] Mirco Natali,[e]* Mariachiara Pastore,[f*] Vincent Artero [b]* and Albert Ruggi [a]*

H_2 evolution catalyzed by a heptacoordinate complex under both electro- (**1**) and photo-chemical (**2**) conditions is analyzed in detail in order to get insights into the mechanism of the processes. The complex shows high catalytic activity for hydrogen production in acetonitrile, in the presence of trifluoroacetic acid and triethylammonium tetrafluoroborate as proton sources. Foot-of-the-wave analysis (FOWA) and Tafel plot analysis have been applied to elucidate the kinetics of the hydrogen evolution mechanism and to benchmark the catalytic performances, respectively, with remarkably high rates being obtained at the expenses of high overpotentials. Transient absorption spectroscopy measurements have been performed to characterize the kinetics and relevant intermediates formed under photocatalytic conditions. A computational investigation, based on density functional theory (DFT) and time-dependent DFT (TD-DFT), is also carried out to characterize the intermediate species and support the experimental results. Combination of both experimental and theoretical data suggests the formation of catalytic intermediates displaying dangling pyridine groups in both the one- and two-electron reduced species, possibly acting as proton-transfer relays to enable efficient H-H bond formation.

1. Introduction

Defining the mechanism behind a reaction is crucial in the quest for the improvement and development of processes such as hydrogen production. Hydrogen plays a primary role in the thrilling and arduous challenge of replacing fossil fuels with renewable and clean sources of energy. In fact, the light-driven reduction of water to H_2 by sunlight is a promising way to store solar energy in the form of chemical bonds since hydrogen can be used as green fuel and its combustion releases a large amount of energy (120 MJ Kg^{-1}).[1,2] This process takes inspiration from natural photosynthesis where microalgae and cyanobacteria carry out the production of hydrogen using hydrogenases enzymes based on nickel and/or iron clusters.[3, 4] In artificial photosynthesis, the light is used to extract electrons from water, resulting in O_2 evolution, and the photogenerated electrons are used to reduce CO_2, to produce organic fuels or to reduce protons to H_2 (i.e. light-driven water splitting).[5] In light-driven water splitting, the half-reaction involving the reduction of protons is widely studied and it has been object of great interest in the last decade.[6] The photochemical production of H_2 requires a multicomponent system based on at least three components: a photosensitizer which is responsible for light-harvesting and the consequent primary photoinduced electron transfer processes, an electron donor which provides the reducing equivalents to foster the photochemical reaction, and a hydrogen evolving catalyst (HEC) capable of stepwise storing electrons and binding protons to promote hydrogen formation at low activation energy.[7] Numerous synthetic noble metal-free catalysts based on Co,[8-10] Ni,[11-13] Fe[14] and Mo[15] have been developed so far for photochemical H_2 production. Among these catalysts, polypyridyl cobalt complexes are considered the most promising ones because of the robustness of the coordination sphere, the possibility of operating in fully aqueous conditions and their high efficiency.[16] In 2011, Chang, Long and co-workers reported the first series of Co complexes coordinated with pentapyridyl ligands, based on pyridine units that were investigated in water in the presence of ascorbic acid as the sacrificial electron donor and $Ru(bpy)_3^{2+}$ (where bpy = 2,2'-bipyridine) as the photosensitizer.[17] Chang, Long, Castellano and co-workers[18] synthesized also another type of pentadentate ligand containing redox-active 2,2'-bipyridine moieties that were expected to stabilize the reduced form of the metal centre. They observed improved activity and stability

of the catalysts attributing the end of the catalysis to the decomposition of the photosensitizer during the photocatalytic process. Another modification was made by Zhao and co-workers,[19] who introduced an alkylamine in the ligand containing pyridine and bipyridine groups. This polypyridyl cobalt complex showed high activity with turnover number (TON) higher than 4400 mol H_2 (mol cat)$^{-1}$ in the presence of $Ru(bpy)_3^{2+}$ and ascorbic acid in water, under optimal conditions. By contrast, Alberto, Probst and co-workers[20] demonstrated that the slight change induced upon replacing a single carbon atom with a nitrogen on the bridge connecting two bipyridyl ligands, causes a reduction of the catalytic rate and of the stability of the catalyst. Another important aspect is the role of the ligand, that can be protonated and therefore can actively participate in the catalytic process as observed for a cobalt pentadentate ligand synthesized by Wang and co-workers[21] and by a recent transient X-ray absorption study.[22] The investigation of the mechanistic profile of each catalyst is imperative for a comprehensive understanding of all the factors that influence the catalytic activity. Cobalt hydrides such as Co(III)-H or Co(II)-H generated from the protonation of Co(I) have been generally acknowledged as the key intermediates for the production of hydrogen, which can occur through either a heterolytic (a proton reacting with a cobalt hydride to evolve H_2) or a homolytic (two cobalt hydrides giving reductive elimination to produce H_2) mechanism. However, it has been proved that the catalytic mechanism could vary depending on the experimental conditions, even for the same system.[16, 23,24]

In our recent work, we reported a new heptacoordinate cobalt complex (Figure 1) and we studied its activity in H_2 photosynthesis using $Ru(bpy)_3^{2+}$ as photosensitizer and ascorbic acid as sacrificial electron donor in aqueous solution.[25] Herein, we go deeper into the investigation of the mechanism, to highlight the pathways of the hydrogen evolution catalysed by this heptacoordinate cobalt complex in electrocatalytic and light-driven systems. The present investigation has been carried out combining evidences obtained by using electrochemistry, transient absorption spectroscopy and quantum chemistry calculations. Concerning the electrochemical studies, foot-of-the-wave analysis (FOWA), bulk electrolysis and catalytic Tafel plot were used to gain information onto the electrocatalytic behaviour of complex **1** (Figure 1) in organic solvent, to shine light onto the operating catalytic mechanism and to benchmark catalytic performances with previously reported systems.[26] Transient absorption spectroscopy has been then exploited to characterize some of the intermediates involved during photocatalytic hydrogen evolution catalysed by complex **2** (Figure 1) in the presence of $Ru(bpy)_3^{2+}$ and ascorbic acid as sensitizer and donor, respectively, and to get information on the kinetics of the relevant electron transfer processes. Density functional theory (DFT) and time-dependent DFT (TD-DFT) calculations have been used to corroborate mechanistic considerations and to characterize the electronic structure and optical response of the possible intermediates involved in the catalysis.

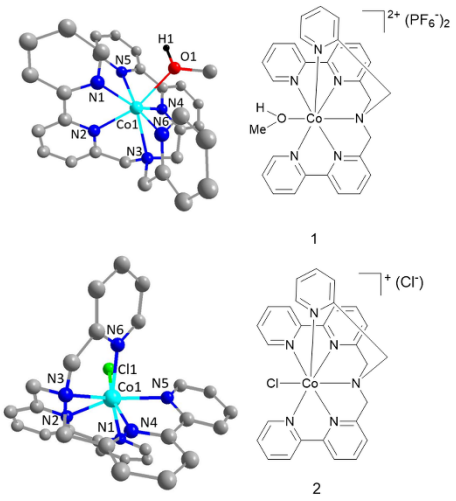

Figure 1 X-ray structures of complex **1** and **2** together with the atom labeling scheme, further details about the structures are in reference. [25]

2. Experimental

2.1 General

All products and solvents were purchased from standard sources and directly used without further purification. Cyclic voltammetry experiments were performed using an *Autolab PGSTAT-30* potentiostat and controlled potential electrolysis experiments were recorded on a *BioLogic SP300* potentiostat. H_2 produced during bulk electrolysis experiments was analysed with a *Perkin-Elmer Clarus 500* gas chromatographer (GC).
The results were validated with at least two sets of measurements.

2.2 Electrochemical investigations

Cyclic voltammograms were recorded in acetonitrile (ACN) in the presence of 0.1 M tetrabutylammonium hexafluorophosphate (nBu$_4$NPF$_6$) as supporting electrolyte under inert atmosphere (N_2). The setup consisted of three electrodes: glassy carbon as working electrode, platinum wire as counter electrode and Ag/AgCl (KCl 3 M) as reference electrode. Ferrocene was used as internal standard.
Controlled potential coulometry experiments were carried out in a two-compartment cell, with the mercury pool working electrode separated by a porous frit from the coiled platinum wire counter electrode. In the working compartment, 8 mL solutions of ACN containing 0.1 M nBu$_4$NPF$_6$, 1 mM catalyst and 100 mM acid (i.e. trifluoroacetic acid (TFA) and triethylammonium tetrafluoroborate (Et_3NHBF_4)) were used for the measurements. Before the measurements, the solutions were degassed with N_2 within 30 minutes and during the experiments the cell was continuously purged with N_2 (5 mL min^{-1}). The headspace was analyzed every two minutes by GC during 4 hours.

2.3 Optical spectroscopy

Emission spectra were taken on an Edinburgh Instrument spectrofluorimeter equipped with a 900 W Xe arc lamp as excitation source, a photomultiplier tube, and an InGaAs detector for the visible and the NIR detection, respectively. Nanosecond transient absorption measurements were performed with a custom laser spectrometer comprised of a Continuum Surelite II Nd:YAG laser (FWHM = 8 ns) with frequency doubled (532 nm, 330 mJ) option, an Applied Photophysics Xe light source including a mod. 720 150 W lamp housing, a mod. 620 power-controlled lamp supply and a mod. 03 - 102 arc lamp pulser. Laser excitation was provided at 90° with respect to the white light probe beam. Light transmitted by the sample was focused onto the entrance slit of a 300 mm focal length Acton SpectraPro 2300i triple grating, flat field, double exit monochromator equipped with a photomultiplier detector (Hamamatsu R3896). Signals from the photomultiplier (kinetic traces) were processed by means of a TeledyneLeCroy 604Zi (400 MHz, 20 GS/s) digital oscilloscope. Before all the measurements the solutions were purged with nitrogen for 10 minutes.

2.4 Computational studies

All the electronic structure calculations have been carried out with the Gaussian09 package,[27] and, following the computational protocol employed in our previous work,[25] the B3LYP functional[28] in combination with a 6-311G** basis set was adopted. Further details are given in ESI.

3. Results and discussion

3.1 Electrochemical characterization

Cyclic voltammetry (CV) of complex **1**, performed at various scan rates in ACN with a glassy carbon electrode and in the presence of tetrabutylammonium hexafluorophosphate (nBu$_4$NPF$_6$) as supporting electrolyte, showed two reversible signals at -1.50 V *vs* Fc$^{+/0}$ and at -2.06 V *vs* Fc$^{+/0}$ (Figure 2 and S3 (ESI)). The B3LYP calculated potentials in ACN corresponding to the two reductions are 3.35 and 2.70 eV (-1.40 and -2.04 V vs Fc$^{+/0}$, respectively), in perfect agreement with the experimental values. Analysis of the β unoccupied orbitals of complex **1** in its high spin electronic configuration (Figure S1**,** left panel) suggests that the first electron likely occupies a mixed Co-bipyridine orbital (BPY1, as indicated in the right panel of Figure S1), while the second electron seems to be completely delocalized on the other bipyridine ligand (BPY2, right panel in Figure S1). Even if it has been observed that standard DFT functionals tend to give too delocalized spin densities in the case of metal-ligand bonds,[29, 30] one can look at the charge (Mulliken) localized on the cobalt centre to get further insights into the nature of the two reductive processes (Table S1), keeping in mind that these values might be underestimated to a certain extent. Complex **1**, with a total charge +2 and in its high spin quartet electronic configuration, presents a calculated Mulliken charge of +1.44 a.u. and a spin density of 2.73 e$^-$ on the metal centre. Upon addition of the first electron (total charge +1 and spin multiplicity of 3), the charge and spin density on the cobalt centre only slightly decrease to +1.39 a.u. and 2.64 e$^-$, respectively. The second electron (complex neutral and spin multiplicity of 2) essentially delocalizes over BPY2 as shown in Figure S1 and by the data in Table S1, leading even to slightly increased charge (+1.41 a.u.) and spin density (2.67 e$^-$) on the cobalt atom. As also shown by the calculated bond distances, the reduction processes involving the two BPY ligands are also accompanied by strengthening between the N-Co bonds of the reduced ligand. Thus, on the basis of DFT calculations, the first reversible cathodic peak can be fairly assigned to the Co$^{II/I}$ metal centered reduction and the second to a ligand centered reduction that involves the bipyridine moieties.

Addition of increasing amounts of TFA in the CV (pK_a = 12.7 in ACN)[31] triggers the appearance of a catalytic wave with a peak current (i_{cat}) that increases with the amount of acid added (Figure 3 and S4). The potential at the mid-wave E_{cat} of -1.46 V *vs* Fc$^{+/0}$, independent of the amount of acid and scan rate (Figure S13), is 40 mV more positive than the reduction potential of Co$^{II/I}$. These observations are consistent with catalysis proceeding via an ECEC process (with E the electron transfer and C the chemical reaction, i.e. the protonation) with the second electron transfer being easier than the first one (Scheme 1a) and the second protonation step being rate-determining.[32]

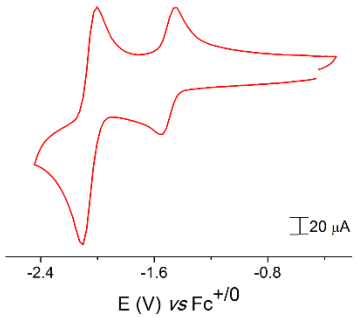

Figure 2 Cyclic voltammogram of complex **1** recorded at 1 V s^{-1} with glassy carbon as working electrode in ACN and 0.1 M nBu$_4$NPF$_6$ supporting electrolyte.

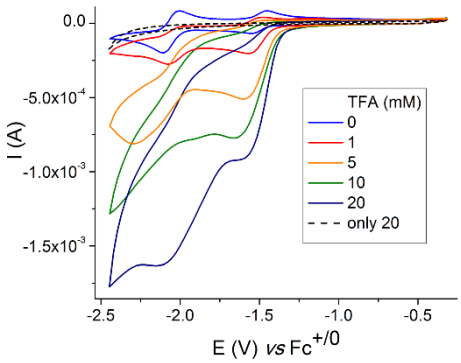

Figure 3 Cyclic voltammograms of complex **1** (1 mM) with increasing amounts of TFA (1-20 mM) in ACN (0.1 M nBu$_4$NPF$_6$, glassy carbon working electrode) at 30 V s^{-1}. The dotted line is obtained at 20 mM of TFA in the absence of complex **1**.

a) $Co(II) \xrightarrow{e^-} Co(I) \xrightarrow{H^+} Co(III)H \xrightarrow{e^-} Co(II)H \xrightarrow{H^+} Co(II) + H_2$ } ECEC

a') $Co(II) \xrightarrow{e^-} Co(I) \xrightarrow{H^+} Co(I)\text{-}BPYH \xrightarrow{e^-} Co(II)H \xrightarrow{H^+} Co(II) + H_2$ } ECEC

b) $Co(II) \xrightarrow{e^-} Co(I) \xrightarrow{e^-} Co(I)\text{-}BPY^- \xrightarrow{H^+} Co(II)H \xrightarrow{H^+} Co(II) + H_2$ } EECC

Scheme 1 Possible pathways for the catalytic hydrogen formation using TFA as the proton source with initial protonation (a) on the metal or (a') on the ligand and (b) using Et_3NH^+ as the proton donor (BPY = BPY1 or BPY2).

Foot-of-the-wave analysis (FOWA), developed by Costentin and Savéant, enables the use of cyclic voltammetry to gain information on the catalytic mechanism and to quantify the rates of the first step during hydrogen evolution.[26]

The plot of i_{cat}/i_p (where i_p is the peak current of a reversible non catalytic wave) versus 1/ (1 + exp (F/RT(E - E_{cat}))) can be linearly fitted near the foot of the catalytic wave. From the slope of such a linear fit it is possible to calculate the rate constant (k_1) of the first protonation process (details about FOWA are provided in the ESI).[32] A value of k_1 = 1.5(±0.2)×10^7 M^{-1}s^{-1} was obtained as average of independent CVs measured at increasing concentrations of TFA (10, 15, and 20 mM) and at five different scan rates (5-50 V s^{-1}).

The rate constant of the rate-determining step in catalysis (k_2) can then be derived from the shift in potential between the catalytic process (mid-wave potential) and the triggering redox couple (here the $Co^{II/I}$ couple) via equation (2) (see ESI).[32, 33] An average value of k_2 = 8.5(±0.7)×10^5 M^{-1}s^{-1} was obtained. A similar value (k_2 = 10.25(±0.05)×10^5 M^{-1}s^{-1}) is independently obtained from the scan-rate independent plateau current observed for 20 mM TFA at 35-40 V s^{-1}.

Catalytic Tafel plots constitute a useful methodology to benchmark the performances of molecular catalysts. Such plots can be outlined from the knowledge of three values characterizing the catalyst: the catalytic potential E_{cat}, the maximum turnover frequency (TOF_{max} = 8.5×10^5 s^{-1} extrapolated to 1 M of acid by convention) and the apparent equilibrium potential of the H^+/H_2 couple (−0.61 V *vs* $Fc^{+/0}$) under such extrapolated conditions.[31, 33-35] To the best of our knowledge, catalytic Tafel plots have never been determined for polypyridyl cobalt catalysts. In Figure 4, the catalytic Tafel plot obtained for complex **1** (blue line) is compared with two known hydrogen evolution catalysts.[35, 36] Catalyst **1** shows high catalytic activity, albeit at the expense of high overpotential values. These properties are common for polypyridyl cobalt catalysts, which are usually known to have higher overpotentials with respect to other cobalt catalysts such as cobaloximes (green plot Figure 4), even though they are more stable and faster in photocatalysis.[20] Similarly, high TOFs correlated with high overpotential have been observed by Bullock, DuBois and co-workers[13] for $[Ni(P_2^{Ph}N^{Ph})_2]^{2+}$ where the well placed proton relays allowed highly fast proton transfer for H_2 formation.[13] At overpotentials higher than 500 mV where

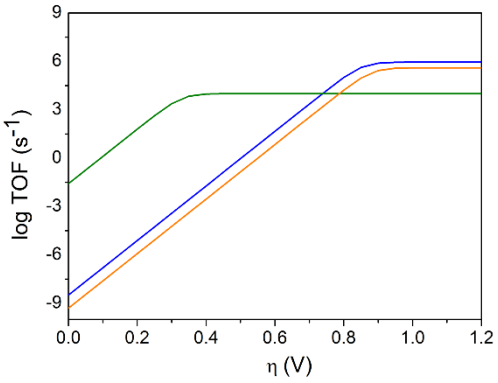

Figure 4 Catalytic Tafel plots. Blue: complex **1** and 1 M of TFA in ACN. Catalysts reported in literature. Green: [Co^{II}(dmgH)$_2$py],[33,35] DMF, Et_3NH^+ (1M); orange: Fe^{II}TPP,[37] DMF, Et_3NH^+(1 M).

log(TOF)/s^{-1} >1 the

activity of catalyst **1** is also comparable to other electrocatalysts such as FeTPP (orange plot Figure 4).[37,36] Bulk electrolysis experiments were performed at -1.53 V *vs* $Fc^{+/0}$ at a mercury pool electrode in the presence of TFA (100 mM) and the catalyst (1 mM) in a solution of ACN for 4h (Figure S11). Production of hydrogen at the catalytic wave was confirmed, with **1** achieving a turnover number (TON) of 21 with a faradaic yield of 75%.

We also investigated the electrochemical behaviour of complex **1** in the presence of the weaker acid Et_3NHBF_4 (pK_a = 18.7 in ACN)[31] (Figure 5). Contrarily to the results obtained with TFA, the catalytic wave was observed at more negative potentials with E_{cat} = -2.06 V *vs* $Fc^{+/0}$, corresponding to the second redox process on the CV recorded in the absence of acid. This observation can be explained considering that Et_3NH^+ may not be able to protonate the Co(I) produced after the first reduction. FOWA analysis of the cyclic voltammograms shown in Figure 5 gives an average value for the first protonation step of k_1 = 2(±0.1)×10^5 M^{-1}s^{-1}. At high scan rate (45 Vs^{-1}) and at 25 mM Et_3NH^+ a k_2 value can be estimated with equation (5) assuming that a scan-rate independent plateauing behaviour is approached under these conditions (Figure S9), giving a value of 5×10^5 M^{-1}s^{-1}. The fact that k_2 is larger than k_1 is coherent with a catalytic EECC process with mid-wave catalytic potential identical to the redox potential of the second redox process observed for complex **1** (Scheme 1b). Bulk electrolysis experiments confirmed the evolution of hydrogen at -2.1 V *vs* $Fc^{+/0}$ with a faradaic yield of 76% and TON of 26 (Figure S12). Of note, a similar reactivity has been observed for NiFe complexes with a Ni-bound bipyridine ligand, with H_2 evolution from Et_3NHBF_4 triggered by a bpy-centred redox process.[38-40] In that case, however, the catalysis took place via a different mechanism, namely with protonation occurring after the two reductive processes (E[ECEC] process with the third electron transfer easier than the second one).

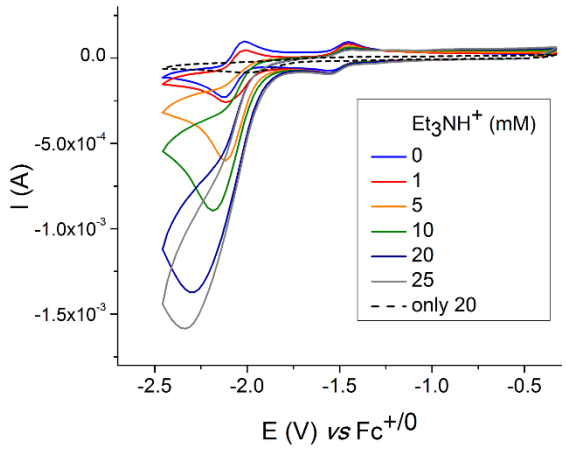

Figure 5 Cyclic voltammograms of complex **1** (1 mM) with increasing amounts of Et_3NH^+ (1-20 mM) in ACN (0.1 M nBu_4NPF_6 glassy carbon working electrode) at 30 V s^{-1}. The dotted line is obtained at 20 mM of Et_3NH^+ in the absence of complex **1**.

3.2 Photochemical characterization

The heptacoordinate complex **2** was found to be efficient in producing hydrogen upon photoirradiation in the presence of $Ru(bpy)_3^{2+}$ as the light-harvesting photosensitizer and ascorbic acid as the sacrificial electron donor. Quantum yields between 3% and 11% were measured in the concentration range of [**2**] = 0.1-10 μM and $Ru(bpy)_3^{2+}$ = 0.5 mM, achieving turnover numbers (TONs) up to 16,300 (±1,600).[25] The remarkable activity observed under strongly diluted conditions clearly suggests that catalyst **2** is effective in undergoing consecutive electron transfer processes from the photogenerated reducing agent. A combination of steady-state and time-resolved techniques has been thus exploited in order to shine light onto the mechanism and kinetics of the three-component photochemical system at the basis of such an efficient hydrogen evolution activity.

In a three-component photochemical system based on a catalyst, a photosensitizer, and a sacrificial electron donor, activation of the catalyst towards hydrogen evolution may be attained through two different mechanisms:[41] i) an oxidative route, where excitation of the sensitizer is followed by photoinduced electron transfer to the catalyst and the oxidized chromophore is recovered back by electron transfer from the donor; ii) a reductive route, in which the sensitizer, upon excitation, undergoes reductive quenching by the donor first and then the photogenerated reduced dye transfers the electron to the catalyst. In order to establish the operating mechanism in photoinduced hydrogen evolution catalysed by **2**, emission measurements have been performed. In 1 M acetate buffer (pH 4) inefficient quenching of the ^{3}*$Ru(bpy)_3^{2+}$ luminescence (< 5% yield) has been observed upon addition of complex **2** up to 10 μM concentration (Figure S15). On the other hand, ascorbic acid is known to quench the triplet excited state of the $Ru(bpy)_3^{2+}$ photosensitizer. However, since the ascorbate anion is the competent quencher, the efficiency of the reductive photoinduced electron transfer is expected to be pH dependent.[42, 43] In 1 M acetate buffer (pH 4) a rate constant of k = 1.0×10^7 $M^{-1}s^{-1}$ has been estimated for such a bimolecular electron transfer reaction.[44] This corresponds to a pseudo-first order rate of 1.0×10^6 s^{-1} and a ca 70% quenching efficiency under the conditions adopted in the light-driven hydrogen evolution experiments (0.1 M ascorbic acid). Overall, these data suggest that photoinduced hydrogen evolution in the three-component system based on **2**, $Ru(bpy)_3^{2+}$, and ascorbic acid in 1 M acetate buffer (pH 4) follows a reductive mechanism. It is worth mentioning that these results are consistent with the typical behaviour observed in other photochemical hydrogen production systems involving the same sensitizer/donor couple and polypyridine cobalt complexes as catalyst.[16]

According to the mechanism outlined above, it is then important to monitor the fate of the photogenerated reduced sensitizer $Ru(bpy)_3^+$ in order to give an estimate of the kinetics of the electron transfer process to catalyst **2** and attain qualitative information on the catalytic intermediate produced. This data can be conveniently obtained by transient absorption spectroscopy in the ns-μs time range on the three-component system. Upon 532-nm excitation of a solution containing 50 μM $Ru(bpy)_3Cl_2{\cdot}6H_2O$, 0.1 M ascorbic acid, and 0.1 mM **2** in 1 M acetate buffer (pH 4) the transient spectrum obtained at 2 μs time-delay (Figure 6) corresponds to the differential spectrum of the reduced sensitizer $Ru(bpy)_3^+$, prepared by reductive quenching of ^{3}*$Ru(bpy)_3^{2+}$ by ascorbic acid, as confirmed by its featuring maximum at ca 500 nm.[45] During the first 10 μs this spectrum decays to give a broad transient signal with maxima at ca 480-500 nm and ca 700 nm (a nice isosbestic point can be seen at ca 575 nm). Interestingly, the kinetics of the $Ru(bpy)_3^+$ decay at 500 nm is dependent on the concentration of catalyst **2** (Figure 6), thus consistent with a bimolecular process involving electron transfer from the photogenerated reduced sensitizer to complex **2**.

Under pseudo-first order kinetic conditions (namely [**2**] >> [$Ru(bpy)_3^+$]), a bimolecular rate constant of k = 2.2(±0.05)×10^9 $M^{-1}s^{-1}$ can be estimated for such an electron transfer process. This rate is considerably high, close to the diffusion-controlled regime and is comparable to the values obtained for the electron transfer from $Ru(bpy)_3^+$ to other cobalt(II) polypyridine complexes.[23, 44, 46-48] It is worth pointing out that fast electron transfer from the photogenerated reduced dye to the catalyst is pivotal in hydrogen evolution photocatalysis in order to minimize parallel, competitive deactivation routes of the chromophore. Accordingly, this peculiar *figure-of-merit* of catalyst **2** may actually explain the achievement of remarkable hydrogen evolution yields as well as the impressive turnover number (TON) experimentally observed during continuous photocatalysis.[25] More importantly, the transient spectrum obtained after the decay of the $Ru(bpy)_3^+$ transient absorption may give also information on the nature of the cobalt species formed upon electron transfer from the photogenerated reduced chromophore. The present transient signal is comparable with the transient spectra experimentally

measured for Co(I) species of related cobalt polypyridine complexes,[46, 48] while apparently differs from that measured for a related Co(III)-H species (with protonation occurring at the metal center).[23] Also, molar extinction coefficients of $\Delta\varepsilon \sim 2{,}300$ and 1,600 $M^{-1}cm^{-1}$ at 500 and 700 nm, respectively, in line with those previously reported for Co(I) intermediates,[48] can be estimated from the transient absorption experiments. Accordingly, these pieces of evidence seem to favor a simple electron transfer pathway over a proton-coupled electron-transfer. Nevertheless, it is worth pointing out that, as suggested by theoretical calculations (see below), the experimental results can also support the hypothesis that, in the present system, one-electron reduction of the cobalt(II) center by photogenerated $Ru(bpy)_3^{+}$ might be coupled to protonation of the ligand.

The transient spectrum formed from the decay of the reduced $Ru(bpy)_3^{+}$, ascribable to the reduced catalyst **2**$^{-}$ (either in the protonated or not protonated form), undergoes decay to the baseline in the 10-100 μs timescale. The kinetics of this decay, followed at 600 nm, is independent of the catalyst concentration and displays well-behaved second-order profiles (Figure 7).

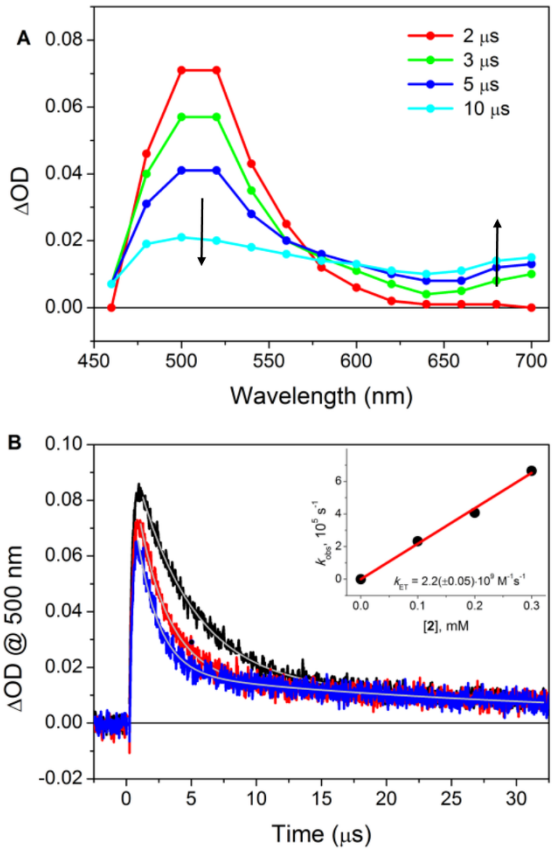

Figure 6 Laser flash photolysis experiments (excitation at 532 nm) of N_2-purged solutions containing 50 μM $Ru(bpy)_3Cl_2{\cdot}6H_2O$, 0.1 M ascorbic acid, and **2** in 1 M acetate buffer (pH 4): A) Spectral evolution between 2-10 μs with 0.1 mM **2**; B) kinetic traces at 500 nm with related fitting in the presence of 0.1 mM (black trace), 0.2 mM (red trace), and 0.3 mM (blue trace) **2**; (inset) plot of the observed rate vs. [**2**] for the estimation of the bimolecular rate constant.

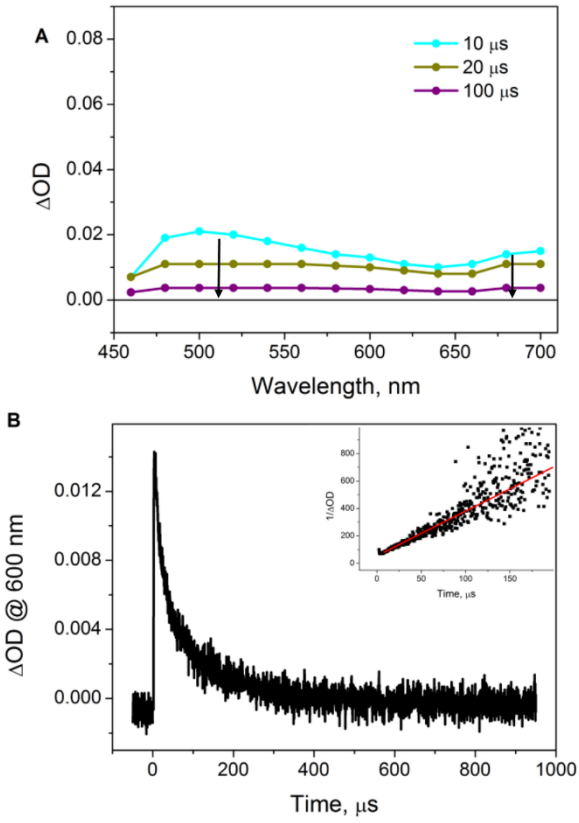

Figure 7 Laser flash photolysis experiments (excitation at 532 nm) of N_2-purged solutions containing 50 μM $Ru(bpy)_3Cl_2.6H_2O$, 0.1 M ascorbic acid, and 0.1 mM **2** in 1 M acetate buffer (pH 4): A) Spectral evolution between 10-100 μs; B) kinetic trace at 600 nm; (inset) second-order kinetic treatment for the estimation of the bimolecular rate constant.

As already shown in similar systems,[48] this process can be reasonably attributed to the bimolecular re-oxidation of the reduced catalyst **2**$^{-}$ by the photogenerated ascorbate radical.

Kinetic treatment of the associated decay allows for the determination of a bimolecular rate constant of $k = 3.9{\times}10^9$ $M^{-1}s^{-1}$ for this process.

The mechanistic information on the three-component photochemical system attained from steady-state and time-resolved studies is summarized in Scheme 2. It should be pointed out that all these processes are bimolecular in nature and thus dependent on the concentration of the species involved.

Accordingly, while the charge recombination processes are efficient in the transient absorption experiments, this cannot be directly extracted to the continuous photolysis conditions.

Firstly, the concentration of these transient species is typically order of magnitudes lower due to the different irradiation power. Secondly, during continuous irradiation subsequent electron and proton transfer to the cobalt complex are expected to take place thus altering the concentration of the corresponding intermediates. Also, competition of the charge recombination reaction with the disproportionation of the ascorbate radical ($k \approx 8{\times}10^7$ $M^{-1}s^{-1}$),[49, 50] at the basis of the "sacrificial" nature of the ascorbic acid electron donor, should be considered.

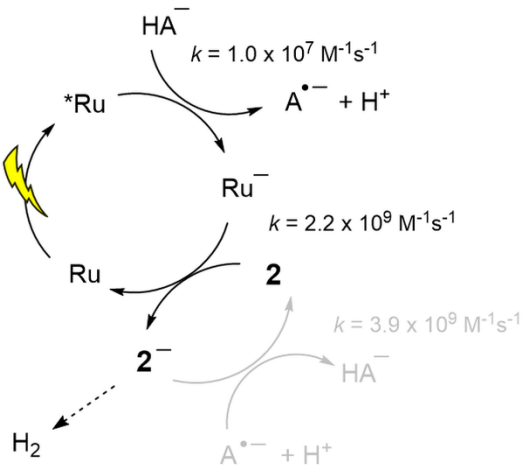

Scheme 2 Primary photoinduced processes with related kinetics for light-driven hydrogen generation by the three-component system based on $Ru(bpy)_3^{2+}$ (Ru) as the photosensitizer, ascorbic acid as the sacrificial electron donor (HA^- and $A^{\bullet-}$ are the ascorbate anion and radical, respectively), and **2** as the catalyst. Forward, favourable processes are shown in black; backward, short-circuiting processes in grey.

3.3 Theoretical calculations

Calculation of UV-Vis absorption spectra of the intermediates are used here to corroborate the transient absorption results discussed above, which suggest the formation of a Co(I) intermediate rather than a Co(III)-H species. The absorption spectra of complex **2** (hereafter Co(II)), the reduced species Co(I) and the three possible protonated reduced species, Co(III)-H (protonation on the metal center), Co(I)-BPY1H and Co(I)-BPY2H (the nomenclature is shown in Figure S1) were calculated using unrestricted TD-DFT (B3LYP) and displayed in the right panel of Figure 8, while some representative (more intense) excitations are listed in Table S2 and analyzed in terms of the associated density difference between the excited and the ground state. In the left panel of Figure 8, the structures of the optimized intermediates are also shown. A first comment concerns the perfect agreement between the experimental absorption spectrum of complex **2** recorded in water (Figure S14) and the calculated one (black line in Figure 8), which shows an intense peak centered at 300 nm and a weak shoulder at around 350 nm.

As listed in Table S2, the intense absorption at 300 nm of complex **2** is dominated by three transitions involving mixed metal-ligand to ligand (MLL') and metal to ligand (ML) excitations, as displayed by the corresponding isodensity plots of the density difference between the excited and the ground state, also displayed in Table S2. The weaker band appearing at ~350 nm is instead ascribable to a pure metal to bipyridine excitation. Compared to complex **2**, the reduced species Co(I) is characterized by a completely different spectral profile (red line in Figure 8), with a less intense but broadened absorption in the UV-Vis region extending up to the NIR and a clear absorption band between 600 and 700 nm. This is in agreement with the measured absorption spectra of a related Co(I) species[23] and nicely supports the assignment of the transient absorption to a Co(I) intermediate. The low energy absorption (600-700 nm) mainly involves excitations from the reduced mixed Co-BPY1 orbital (see the 129 β orbital in Figure S1) toward empty metal-ligand or pure ligand orbitals, as displayed in the density difference isosurface plots associated to the 13th and 14th excited states (Table S2). In the 300-500 nm region, a three-bands profile appears, characterized by mixed MLL', ligand-to-ligand (LL') and inter-ligand (IL) excitations, involving excitations out of the highest occupied α and β orbitals. As shown in Table S2, the charge depletion (red lobes) always involves the reduced BPY1 ligand, while the electron being promoted (blue lobes) to the second BPY2 ligand. A sizeable destabilization (0.6-1.0 eV) of the occupied α and β Kohn-Sham orbitals accompanied by only a minor upshift of the unoccupied ones (0.3-0.4 eV)

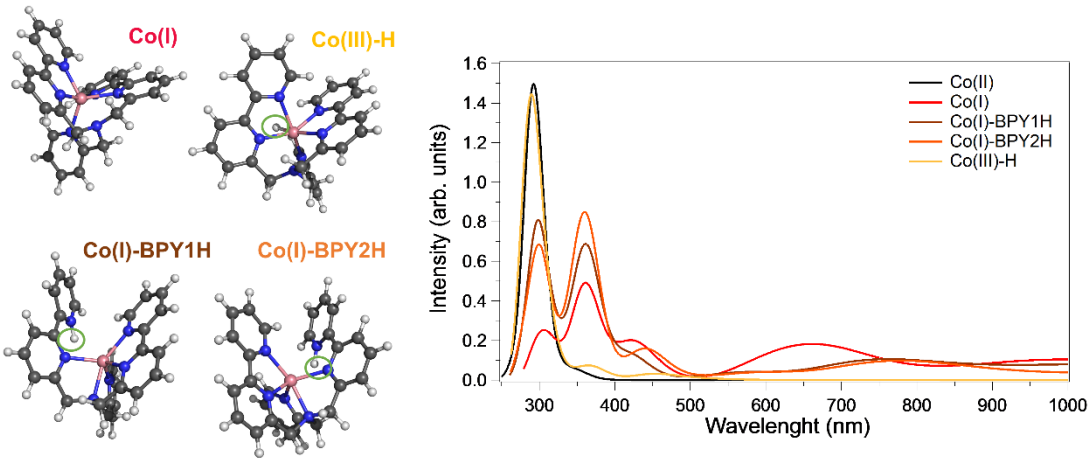

Figure 8 Right: calculated absorption spectra of various intermediates species (Co(I) red line, Co(III)-H yellow line, Co(I)-BPY1H brown line and Co(I)-BPY2H orange line) and of the original catalyst (Co(II) black line); left: optimized ground state structures and labelling of the different intermediates considered.

explains the overall red shift of the absorption spectrum and the absorption in the NIR portion of the spectrum. The protonation of the reduced species at the metal center, i.e. Co(III)-H, completely alters the optical properties of the reduced complex. The absorption spectrum of the Co(III)-H complex (yellow line in Figure 8) closely resembles that of the Co(II), with an intense band appearing around 300 nm. A deeper look at the results reveals that this is the direct consequence of the strong energetic stabilization of the occupied and virtual Kohn-Sham orbitals, whose eigenvalues are close to the ones obtained for the Co(II) species, which follows the protonation process. For the optimized Co(III)-H intermediate in water, the predicted Co-H bond polarization yields a positive charge of 0.25 and 1.38 a.u. on the H and Co atoms, respectively, with a bond distance of 1.467 Å. The two lowest energy peaks at ~450 and ~370 nm (Table S2) are ascribable to excited states having similar nature and characterized by charge transfer from mixed ML orbitals to the H and N (on the bipyridines) atoms (see the density difference plots for states 8 and 11 in Table S2). The higher-energy intense band is instead a complex mixing of different MLL', LL', IL and ML excitations. This result is fully supported by the experimental evidence found for another Co system,[23] since the absorption spectra of Co(II) and Co(III)-H present a coincident band at about 300 nm and Co(III)-H shows also a weak and broadened band at about 480 nm; the absorption spectrum of Co(I) is, on the other hand, completely different, as discussed above.

Besides the protonation of Co(I) complex on the metal, we investigated if protonation could occur on bipyridine ligands associated to partial decoordination. The protonation of the reduced species on the bipyridines (Co(I)-BPY1H and Co(I)-BPY2H), as expected, yields to intermediates showing an absorption profile closely resembling the one of Co(I), with the exception of the absorption band at about 560 nm, that is less intense and shifted at slightly lower energies (ca. 700-800 nm) in the case of the protonated reduced complexes. The Mulliken charge on the metal centre is 1.43 and 1.45 a.u. in the Co(I)-BPY1H and Co(I)-BPY2H, respectively, whereas in both cases a charge of -0.65/+0.38 is calculated for N/H. On the basis of the TD-DFT results, we can thus suggest the formation of a Co(I) intermediate ruling out the appearance of the Co(III)-H hydride intermediate. Finally, the formation of the protonated Co(I)-BPY1H and Co(I)-BPY2H cannot be completely discarded, considering the similar absorption properties in the 600-800 nm region (see red, orange and brown lines in Figure 8).

3.4 Mechanistic considerations

Energetic considerations, based on the relative free energy changes associated with the formation of various intermediates along the reaction (Table S3 and Figure 9), also seem to rule out the formation of Co(III)-H. In fact, the direct protonation of the metal centre in Co(I) implies a ΔG of +13.5 Kcal/mol, whilst the protonation of one of the bipyridine moieties is almost thermodynamically costless (see Figure 9). Interestingly, the second reduction/protonation, leads to three close in energy, although structurally different, intermediates (see Figure 9):

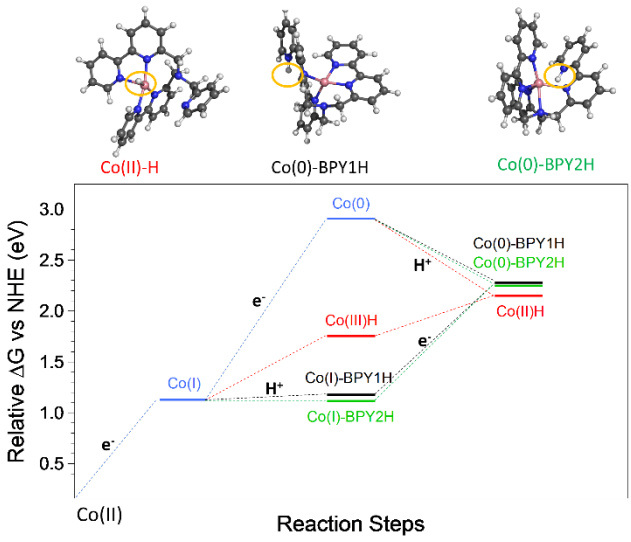

Figure 9 Top: optimized molecular structure of the three possible intermediates after the two reductions and the protonation steps. Bottom: calculated free energies differences (in eV) in acetonitrile for the possible reaction steps involved in the proposed mechanism.

Co(II)-H, having the proton on the Cobalt, and the two possible Co(0)-BPYH intermediates, having one of the two bipyridines in a protonated form. As to the Co(II)-H intermediate, the calculated Mulliken charge in solution on the Co atom is 1.16 a.u with a spin density of 1.10; the H atom bonded to the metal (Co-H 1.53 Å) has calculated charge of -0.42 a.u., clearly indicating that the Co-H bond is accepting almost the totality of the second electron (about 0.2 and 0.5 e- on the metal and H, respectively). As is apparent in Figure 9, important structural changes involve the metal coordination sphere, with dissociation of the Co-$N_{pyridine}$ bond (3.80 Å) and a strong elongation of the Co-N_{amine} bond (2.75 Å). Considering the pKa of pyridine in water (pK_a = 5.3), protonation of the pendent pyridine is expected to occur at acidic pH resulting in a favourable proton relay for facilitating H-H bond formation,[13, 42] as recently proposed by Smolentsev and co-workers for a similar Co-based polypyridyl catalyst.[22] The other two possible intermediates originated by the reduction of the two Co(I)-BPYH species have a positive charge of 1.38 a.u. on the Cobalt centre, indicating that only a very small fraction of the second electron reduces the metal, while, as expected, it largely delocalizes on the bi-coordinated BPY ligand that is not protonated. The charge on the nitrogen atoms (N4 and N5 for Co(0)-BPY1H and N1 and N2 for Co(0)-BPY2H, labelling in Figure S1) are indeed between -0.65 and -0.72 a.u. and Co-N bond distances comprised between 1.98 and 2.07 Å. Even in this option, the presence of a protonated BPY ligand produces pendent N bases which possibly plays the role of proton relay for the H_2 evolution step.

In summary, DFT calculations suggest that hydrogen evolution catalyzed by the heptadentate Co(II) complex involves a first reduction/protonation step generating Co(I)-BPY1H or Co(I)-BPY2H intermediates featuring a reduced metal centre and a protonated ligand. These intermediates are indeed expected to

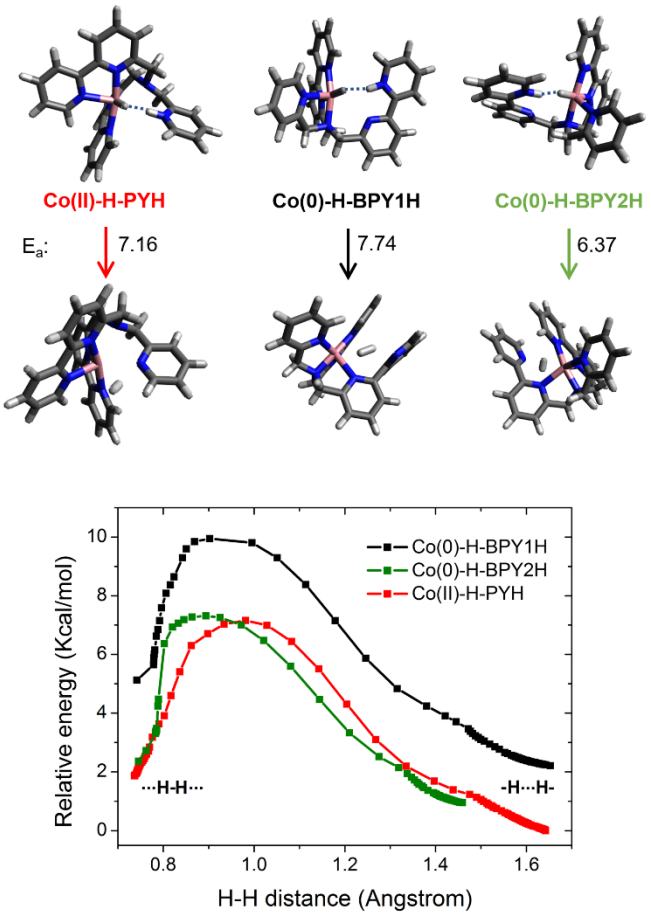

Figure 10 Right: Minimum energy path of the doubly protonated species from their respective minima (–H···H–) to H_2 formation (···H–H···) as a function of the hydrogen interatomic distance. Left: Initial (top) and final (bottom) structures of the minimum energy paths, including the required activation energy barrier (E_a) in kcal/mol.

be more stable than the one attainable by direct protonation of the metal centre (namely Co(III)-H). This evidence is consistent with the experimental results obtained by transient absorption spectroscopy, which showed that the reduction of catalyst **2** by the photogenerated $Ru(bpy)_3^+$ reducing agent brings to the formation of a catalytic intermediate **2**$^-$. Such an intermediate can in fact be unambiguously assigned to a Co(I) species and be thus compatible with both Co(I)-BPY1H and Co(I)-BPY2H. Moreover, these considerations might also support the observation that in the electrochemical experiments the first EC process (namely reduction/protonation) from the cobalt(II) species occurs only when trifluoroacetic acid is used as the proton source. As a matter of fact, protonation of the pendent pyridine in Co(I)-BPY (pK_a = 12.5 for pyridine in acetonitrile)[51] might be thermodynamically feasible using TFA (pK_a = 12.7 in acetonitrile),[51] while being potentially up-hill employing Et_3NH^+ (pK_a = 18.8 in acetonitrile).[51] An additional reduction step is indeed required in this latter instance to allow protonation (EEC process).

As to the second reduction of the purported Co(I)-BPY1H or Co(I)-BPY2H intermediates formation of Co(0)-BPY1H and Co(0)-BPY2H species are envisioned at first glance. It is however plausible to hypothesize that these species could be converted into the isoenergetic derivative Co(II)-H featuring a dangling pyridine moiety. Within this hypothesis the presence of a pendent N base in the doubly-reduced and protonated form could easily assist the eventual H-H bond formation. To this respect, the intrinsic ability of the catalyst to provide suitable proton relays in the singly- and doubly-reduced state represents a peculiar property of this class of catalysts and may potentially explain the high turnover frequencies measured under electrochemical conditions as well as the high quantum efficiencies observed in light-driven hydrogen evolution.[25]

To support this hypothesis, calculations were performed to establish the limiting step to convert Co(0)-H-BPY1/2H into Co(II)-H, corresponding to the proton transfer from bipyridine to the metal centre (see ESI). The energy barrier (27-28 kcal/mol) agrees well with previously reported molecular catalysts.[52-54] Furthermore, the possible generation of H_2, after protonation of the pyridine (Co(II)-H-PYH) or the Co centre (Co(0)-H-BPY1H and Co(0)-H-BPY2H), was studied in detail by calculating their respective minimum energy path (Figure 10). In all three cases, a highly feasible energy barrier (6-8 kcal/mol) was found, with the newly formed H_2 molecule almost released from the complex.

4. Conclusions

In this work, we have reported a detailed mechanistic study on a recently synthesized cobalt catalyst based on a hexadentate polypyridyl ligand that displays high activity for photoinduced hydrogen production in water. The electrochemical investigation in CH_3CN elucidated the kinetics of the catalytic process in the presence of TFA or Et_3NH^+ as proton sources. Remarkably high rates have been observed, although at the expenses of high overpotentials. Transient absorption studies and theoretical calculations showed that hydrogen evolution occurs via a series of electron and proton transfer processes involving formation of two relevant intermediates. The first one (Co(I)-BPY1H or Co(I)-BPY2H) is obtained upon electron transfer at the metal centre followed by protonation at the ligand, the second one (most plausibly Co(II)-H with a dangling pyridine) upon further electron transfer and protonation of the metal centre. Within this picture, the presence of extended coordination sites based on multidentate polypyridyl ligands, besides providing a stable coordination environment to the cobalt centre, plays a beneficial role in the catalytic mechanism by supplying suitable relays for promoting intramolecular proton transfer processes. Further studies including modifications of the ligands with different groups in the peripheral position to promote intramolecular proton transfer are currently in progress.

Conflicts of interest

There are no conflicts to declare.

Acknowledgements

F.L. and A.R. thank the Swiss National Foundation (Grant FN 7359) for the generous financial support. M.P. thanks Dr. Francesca Ingrosso for fruitful discussions and HPC resources from GENCI-CCRT/CINES (Grants 2018-A0010810139) and from the LPCT local computing clusters. M.M. acknowledges Universidad de Alcalá for a postdoctoral contract. M.N. acknowledges the University of Ferrara (FAR2018) for funding. This work was also supported by the French National Research Agency within grant ANR JCJC HELIOSH2 (ANR-17-CE05-0007-01), the Labex program ARCANE (ANR-11-LABX-0003-01) and CBH-EUR-GS (ANR-17-EURE-0003).

References

1. D. Stolten, ed., *Hydrogen and Fuel Cells: Fundamentals, Technologies and Applications*, Wiley-VCH 2010.
2. V. Balzani, A. Credi and M. Venturi, *ChemSusChem*, 2008, **1**, 26-58.
3. J. C. Fontecilla-Camps, A. Volbeda, C. Cavazza and Y. Nicolet, *Chem. Rev.*, 2007, **107**, 4273-4303.
4. S. T. Stripp and T. Happe, *Dalton Trans.*, 2009, 9960-9969.
5. J. Barber, *Chem. Soc. Rev.*, 2009, **38**, 185-196.
6. Z. Han and R. Eisenberg, *Accounts Chem. Res.*, 2014, **47**, 2537-2544.
7. W. T. Eckenhoff and R. Eisenberg, *Dalton Trans.*, 2012, **41**, 13004-13021.
8. X. Hu, B. M. Cossairt, B. S. Brunschwig, N. S. Lewis and J. C. Peters, *Chem. Commun.*, 2005, 4723-4725.
9. V. Artero, M. Chavarot-Kerlidou and M. Fontecave, *Angew. Chem. Int. Ed.*, 2011, **50**, 7238-7266.
10. M. Razavet, V. Artero and M. Fontecave, *Inorg. Chem.*, 2005, **44**, 4786-4795.
11. Y. A. Small, D. L. DuBois, E. Fujita and J. T. Muckerman, *Energy Environ. Sci.*, 2011, **4**, 3008-3020.
12. T. Straistari, J. Fize, S. Shova, M. Réglier, V. Artero and M. Orio, *ChemCatChem*, 2017, **9**, 2262-2268.
13. M. L. Helm, M. P. Stewart, R. M. Bullock, M. R. DuBois and D. L. DuBois, *Science*, 2011, **333**, 863-866.
14. S. Kaur-Ghumaan, L. Schwartz, R. Lomoth, M. Stein and S. Ott, *Angew. Chem., Int. Ed.*, 2010, **49**, 8033-8036.
15. H. I. Karunadasa, C. J. Chang and J. R. Long, *Nature*, 2010, **464**, 1329.
16. N. Queyriaux, R. T. Jane, J. Massin, V. Artero and M. Chavarot-Kerlidou, *Coordin. Chem. Rev.*, 2015, **304**, 3-19.
17. Y. Sun, J. P. Bigi, N. A. Piro, M. L. Tang, J. R. Long and C. J. Chang, *J. Am. Chem. Soc.*, 2011, **133**, 9212-9215.
18. M. Nippe, R. S. Khnayzer, J. A. Panetier, D. Z. Zee, B. S. Olaiya, M. Head-Gordon, C. J. Chang, F. N. Castellano and J. R. Long, *Chem. Sci.*, 2013, **4**, 3934-3945.
19. W. M. Singh, T. Baine, S. Kudo, S. L. Tian, X. A. N. Ma, H. Y. Zhou, N. J. DeYonker, T. C. Pham, J. C. Bollinger, D. L. Baker, B. Yan, C. E. Webster and X. Zhao, *Angew. Chem. Int. Ed.*, 2012, **51**, 5941-5944.
20. S. Schnidrig, C. Bachmann, P. Muller, N. Weder, B. Spingler, E. Joliat-Wick, M. Mosberger, J. Windisch, R. Alberto and B. Probst, *ChemSusChem*, 2017, **10**, 4570-4580.
21. J. P. Bigi, T. E. Hanna, W. H. Harman, A. Chang and C. J. Chang, *Chem. Commun.*, 2010, **46**, 958-960.
22. G. Smolentsev, M. A. Soldatov, B. Probst, C. Bachmann, N. Azzaroli, R. Alberto, M. Nachtegaal and J. A. van Bokhoven, *ChemSusChem*, 2018, **11**, 3087-3091.
23. A. Lewandowska-Andralojc, T. Baine, X. Zhao, J. T. Muckerman, E. Fujita and D. E. Polyansky, *Inorg. Chem.*, 2015, **54**, 4310-4321.
24. S. C. Marinescu, J. R. Winkler and H. B. Gray, *Proc. Natl. Acad. Sci. U.S.A.* , 2012, **109**, 15127-15131.
25. F. Lucarini, M. Pastore, S. Vasylevskyi, M. Varisco, E. Solari, A. Crochet, K. M. Fromm, F. Zobi and A. Ruggi, *Chem. Eur. J.*, 2017, **23**, 6768-6771.
26. C. Costentin, S. Drouet, M. Robert and J. M. Saveant, *J. Am. Chem. Soc.*, 2012, **134**, 11235-11242.
27. C. J. Adamo, J.; Gomperts, R.; Stratmann, R. E.; Yazyev, O.; Austin, A. J.; Cammi, R.; Pomelli, C.; Ochterski, J. W.; Martin, R. L.; et al, *Gaussian 09, Revision D.01, Gaussian, Inc., Wallingford CT, 2013.*, 2013.
28. A. D. Becke, *J. Chem. Phys.*, 1993, **98**, 5648-5652.
29. E. Giner and C. Angeli, *J. Chem. Phys.*, 2015, **143**.
30. M. Pastore, F. De Angelis and C. Angeli, *Theor. Chem. Acc.*, 2016, **135**, 108.
31. C. Baffert, V. Artero and M. Fontecave, *Inorg. Chem.*, 2007, **46**, 1817-1824.
32. C. Costentin and J. M. Saveant, *ChemElectroChem*, 2014, **1**, 1226-1236.
33. V. Artero and J. M. Saveant, *Energy Environ. Sci.*, 2014, **7**, 3808-3814.
34. V. Fourmond, P. A. Jacques, M. Fontecave and V. Artero, *Inorg. Chem.*, 2010, **49**, 10338-10347.
35. N. Coutard, N. Kaeffer and V. Artero, *Chem. Commun.*, 2016, **52**, 13728-13748.
36. I. Bhugun, D. Lexa and J.-M. Savéant, *J. Am. Chem. Soc.*, 1996, **118**, 3982-3983.
37. V. Artero and J.-M. Saveant, *Energy Environ. Sci.*, 2014, **7**, 3808-3814.
38. D. Brazzolotto, L. K. Wang, H. Tang, M. Gennari, N. Queyriaux, C. Philouze, S. Demeshko, F. Meyer, M. Orio, V. Artero, M. B. Hall and C. Duboc, *ACS Catal.*, 2018, **8**, 10658-10667.
39. D. Brazzolotto, M. Gennari, N. Queyriaux, T. R. Simmons, J. Pecaut, S. Demeshko, F. Meyer, M. Orio, V. Artero and C. Duboc, *Nat. Chem.*, 2016, **8**, 1054-1060.
40. H. Tang and M. B. Hall, *J. Am. Chem. Soc.*, 2017, **139**, 18065-18070.
41. W. T. Eckenhoff, *Coord. Chem. Rev.*, 2018, **373**, 295-316.
42. A. Reynal, E. Pastor, M. A. Gross, S. Selim, E. Reisner and J. R. Durrant, *Chem. Sci.*, 2015, **6**, 4855-4859.
43. M. Natali, *ACS Catal.*, 2017, **7**, 1330-1339.
44. E. Deponti, A. Luisa, M. Natali, E. Iengo and F. Scandola, *Dalton Trans.*, 2014, **43**, 16345-16353.
45. L. A. Kelly and M. A. J. Rodgers, *J. Phys. Chem.*, 1994, **98**, 6377-6385.
46. R. S. Khnayzer, V. S. Thoi, M. Nippe, A. E. King, J. W. Jurss, K. A. El Roz, J. R. Long, C. J. Chang and F. N. Castellano, *Energy Environ. Sci.*, 2014, **7**, 1477-1488.
47. M. Natali, E. Badetti, E. Deponti, M. Gamberoni, F. A. Scaramuzzo, A. Sartorel and C. Zonta, *Dalton Trans.*, 2016, **45**, 14764-14773.
48. W. M. Singh, M. Mirmohades, R. T. Jane, T. A. White, L. Hammarström, A. Thapper, R. Lomoth and S. Ott, *Chem. Commun.*, 2013, **49**, 8638-8640.

49. B. H. J. Bielski, D. A. Comstock and R. A. Bowen, *J. Am. Chem. Soc.*, 1971, **93**, 5624-5629.
50. G. M. Brown, B. S. Brunschwig, C. Creutz, J. F. Endicott and N. Sutin, *J. Am. Chem. Soc.*, 1979, **101**, 1298-1300.
51. I. Kaljurand, A. Kütt, L. Sooväli, T. Rodima, V. Mäemets, I. Leito and I. A. Koppel, *J. Org. Chem.*, 2005, **70**, 1019-1028.
52. A. Bhattacharjee, E. S. Andreiadis, M. Chavarot-Kerlidou, M. Fontecave, M. J. Field and V. Artero, *Chem. Eur. J.*, 2013, **19**, 15166-15174.
53. E. J. Sundstrom, X. Yang, V. S. Thoi, H. I. Karunadasa, C. J. Chang, J. R. Long and M. Head-Gordon, *J. Am. Chem. Soc.*, 2012, **134**, 5233-5242.
54. L. Ridder, A. J. Mulholland, J. Vervoort and I. M. C. M. Rietjens, *J. Am. Chem. Soc.*, 1998, **120**, 7641-7642.